


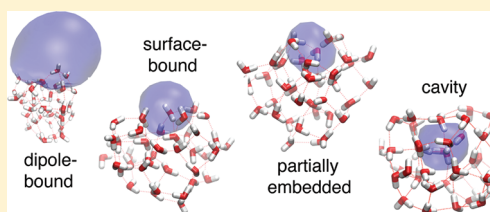
# Theoretical Characterization of Four Distinct Isomer Types in Hydrated-Electron Clusters, and Proposed Assignments for Photoelectron Spectra of Water Cluster Anions

Leif D. Jacobson<sup>†</sup> and John M. Herbert<sup>\*</sup>

Department of Chemistry, The Ohio State University, Columbus, Ohio 43210, United States

 Supporting Information

**ABSTRACT:** Water cluster anions,  $(\text{H}_2\text{O})_N^-$ , are examined using mixed quantum/classical molecular dynamics based on a one-electron pseudopotential model that incorporates many-body polarization and predicts vertical electron detachment energies (VDEs) with an accuracy of  $\sim 0.1$  eV. By varying the initial conditions under which the clusters are formed, we are able to identify four distinct isomer types that exhibit different size-dependent VDEs. On the basis of a strong correlation between the electron's radius of gyration and its optical absorption maximum, and extrapolating to the bulk limit ( $N \rightarrow \infty$ ), our analysis supports the assignment of the "isomer Ib" data series, observed in photoelectron spectra of very cold clusters, as arising from cavity-bound  $(\text{H}_2\text{O})_N^-$  cluster isomers. The "isomer I" data reported in warmer experiments are assigned to surface-bound isomers in smaller clusters, transitioning to partially embedded isomers in larger clusters. The partially embedded isomers are characterized by a partially formed solvent cavity at the cluster surface, and they are spectroscopically quite similar to internalized cavity isomers. These assignments are consistent with various experimental data, and our theoretical characterization of these isomers sheds new light on a long-standing assignment problem.



## 1. INTRODUCTION

**1.1. Motivation and Significance.** The aqueous electron,  $e^-(\text{aq})$ , is formed by radiolysis or high-intensity UV irradiation of liquid water.<sup>1</sup> Although first detected nearly half a century ago,<sup>2</sup> many fundamental questions remain regarding the precise chemical identity, characteristics, and behavior of this species.<sup>3</sup> For example, the long-held belief<sup>4–6</sup> that  $e^-(\text{aq})$  is stabilized by cavity formation in the solvent has recently been questioned,<sup>7</sup> and debate on this subject continues.<sup>8–11</sup> One key aspect of interest is to elucidate the dynamics prior to full equilibration of  $e^-(\text{aq})$ , or in other words, to ask the question: how does the electron get there? Another fundamental question is how strongly the electron is solvated, that is, what is the electron affinity of liquid water? These questions are not entirely academic; the hydrated electron has been implicated in DNA damage,<sup>12–14</sup> and is an important intermediate in the chemistry of nuclear reactors and nuclear waste.<sup>1</sup>

Anionic water clusters,  $(\text{H}_2\text{O})_N^-$ , are finite-sized analogues of the aqueous electron, and might be thought to offer simplified models of  $e^-(\text{aq})$ . By systematically increasing the size of such clusters, one can investigate solvation as it evolves toward the bulk limit. First observed by Haberland and co-workers in the early 1980s,<sup>15,16</sup>  $(\text{H}_2\text{O})_N^-$  clusters have since been studied intensely by theorists and experimentalists alike. One can measure, and in some cases, calculate with high accuracy, the properties of clusters, then extrapolate these properties to  $N = \infty$ . However, an ongoing controversy regarding the electron binding motifs in  $(\text{H}_2\text{O})_N^-$  clusters has cast some doubt on the validity of any extrapolations.

A complete review of this topic is beyond the scope of this report, but a synopsis of previous work on  $(\text{H}_2\text{O})_N^-$  clusters is presented below.

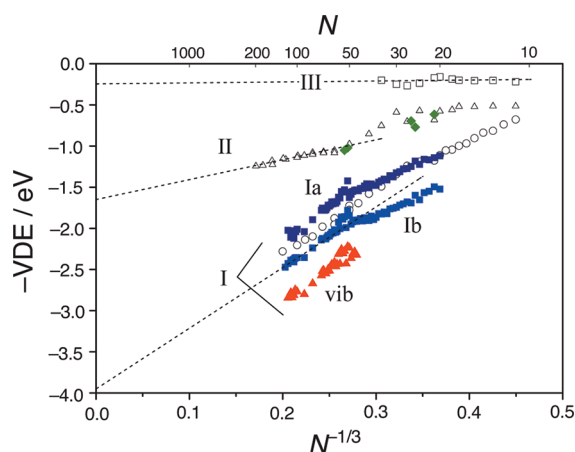
**1.2. Historical Background.** In the late 1980s, Barnett et al.<sup>17–19</sup> used path integral molecular dynamics simulations, in conjunction with an electron–water pseudopotential,<sup>18</sup> to show that a water cluster can accommodate an extra electron either in a surface-binding motif or else within the interior of the cluster.<sup>19</sup> This theoretical work represented the first suggestion that it might be possible to observe two distinct isomeric species in a molecular beam experiment. For cluster isomers consisting of an internalized electron, the vertical electron detachment energy (VDE),

$$\text{VDE} = E(\text{anion}) - E(\text{neutral}) \quad (1)$$

was found to increase with cluster size as  $N^{-1/3}$ . This trend was explained using a Born-type continuum model consisting of an electron localized within a cavity of fixed size that is carved out of a spherical dielectric medium whose radius grows as  $N^{1/3}$ .<sup>19</sup> Isomers in which the extra electron is bound to the cluster surface were found to be more stable for  $N \leq 32$ , whereas for  $N = 64$  and  $N = 128$ , the internalized isomers were found to be more stable. This work first established the notion of a surface  $\rightarrow$  internal transition in  $(\text{H}_2\text{O})_N^-$  clusters at some finite  $N$ , and further instilled the

Received: August 24, 2011

Published: October 25, 2011



**Figure 1.** Experimental vertical detachment energies (VDEs) for size-selected  $(\text{H}_2\text{O})_N^-$  anions, from cluster photoelectron spectroscopy. The unfilled symbols represent data from Verlet et al.,<sup>25</sup> who labeled their observed isomer series as I, II, and III. (We will refer to the open circles as “isomer I”, consistent with the labels in ref 25.) The filled, colored symbols represent data from Ma et al.,<sup>28</sup> who labeled two of their data series as Ia and Ib, and assigned the third series (“vib”) to vibrational excitation of an O–H stretch upon photodetachment of the electron. The broken lines are tentative extrapolations from ref 28. Figure reprinted with permission from ref 28. Copyright 2009 American Institute of Physics.

notion of the internalized isomers as consisting of “cavity-bound” electrons.

A short time later, photoelectron spectra of cluster isomers up to  $N = 69$  were reported by Coe et al.,<sup>20</sup> who observed a linear trend in VDE as a function of  $N^{-1/3}$ . Extrapolation to  $N = \infty$  afforded a VDE of  $\approx 3.3$  eV,<sup>21</sup> which was interpreted as an estimate of the VDE of  $e^-(\text{aq})$  in bulk water. Interestingly, however, the VDEs computed by Barnett et al. for surface states better matched the data of Coe et al. than did the computations for internally bound electrons. Later, Makov and Nitzan<sup>22</sup> showed that dielectric continuum theory could be used to obtain  $N^{-1/3}$  scaling of the VDE for both surface and cavity states, provided the cluster radius is large compared to the electron’s radius of gyration. As such, the scaling observed experimentally by Coe et al. is insufficient to conclude that the isomers interrogated in those experiments are indeed cavity-bound.

The VDE is not the only relevant experimental observable, and Barnett et al.<sup>23</sup> have also noted, using both simulations and dielectric continuum theory, that the optical absorption maximum for surface-bound  $(\text{H}_2\text{O})_N^-$  isomers steadily blue-shifts with increasing cluster size, whereas the absorption maximum for cavity states is converged to the bulk limit even in small clusters. In 1997, Ayotte and Johnson<sup>24</sup> measured these spectra for clusters ranging from  $N = 6$  to  $N = 50$  and found that the spectra are strongly red-shifted compared to the bulk  $e^-(\text{aq})$  absorption maximum. The experimental spectra blue-shift with increasing cluster size, and an  $N^{-1/3}$  extrapolation accurately reproduces the location of the bulk  $e^-(\text{aq})$  absorption maximum.<sup>24</sup>

In 2005, Verlet et al.<sup>25</sup> discovered that by varying the source conditions of their cluster expansion, three distinct populations of isomers could be identified whose relative populations could be modulated continuously as a function of the backing pressure of the carrier gas. At higher backing pressures, corresponding to lower temperature, two new series of isomers were identified,

having VDEs lower than those observed by Coe et al.<sup>20</sup> In all, three series of isomers were observed for  $11 \leq N \leq 200$  and were labeled I, II, and III (see Figure 1), with  $\text{VDE}_I > \text{VDE}_{II} > \text{VDE}_{III}$ .<sup>25</sup> The isomer I data of Verlet et al. nearly coincide<sup>14,26</sup> with the earlier data reported by Coe et al., and match up with the  $N \leq 11$  photoelectron data of Johnson and co-workers.<sup>27</sup> The weaker-binding isomers II and III, which are observed only at colder temperatures, were assigned by Verlet et al. to surface-bound electrons, whereas isomer I was assigned as the internally bound species.

This interpretation was quickly challenged by Turi et al.,<sup>29</sup> based on quantum/classical molecular dynamics simulations using a new pseudopotential model.<sup>30</sup> In these simulations, cavity-bound isomers of  $(\text{H}_2\text{O})_N^-$  are not thermodynamically stable for  $N \leq 100$ , although they may be kinetically trapped at low temperature. The absorption maxima computed for cavity isomers exhibits no blue-shift with cluster size in these simulations, leading Turi et al. to argue that only surface-bound isomers had been observed experimentally,<sup>29,31</sup> since absorption spectra for clusters prepared under conditions similar to those that yield isomer I are found to blue-shift with cluster size.<sup>24</sup> It is worth noting, however, that VDEs computed by Turi et al. for the cavity-bound isomers are in better agreement with the experimental isomer I data than are VDEs computed for the surface-bound isomers.<sup>32</sup>

For very small clusters ( $N \leq 7$ ), the identity of the cluster isomers observed experimentally is less ambiguous thanks to infrared spectra obtained by Johnson and co-workers,<sup>33–37</sup> which can be assigned to specific isomers based on ab initio calculations.<sup>34,36–38</sup> It is found that the so-called “double acceptor” or “AA” binding motif, in which the electron binds most directly to a water molecule that accepts two hydrogen bonds and donates none, is pervasive. (Interestingly, although the AA isomers appear to dominate the experimental spectra, they are typically *not* the lowest-energy isomers at a given cluster size.<sup>39,40</sup>) Subsequent experiments suggested that the AA structural motif persists up to at least  $N = 24$ .<sup>41,42</sup> These findings seem to support the assignment of isomer I as a surface-bound species, in concurrence with the thesis of Turi et al.<sup>29</sup> However, Neumark and co-workers have pointed out that the photoelectron data for isomer I change slope around  $N = 30$ , which suggests that some structural change may occur in this regime.<sup>36,43</sup> Furthermore, the AA-bending feature in the infrared spectrum shifts and broadens from  $N = 25$  to  $N = 50$ , which may indicate a transition from a binding motif that involves primarily a single water molecule (the AA) to a motif that is characterized by collective solvation of the excess electron.<sup>43</sup>

More recently, Ma et al.<sup>28</sup> reported photoelectron spectra of very cold  $(\text{H}_2\text{O})_N^-$  clusters ( $T \sim 10$  K). In addition to observing a few data points that seem to match isomer II, these experiments identified two new series of high-binding isomers (denoted “Ia” and “Ib”; see Figure 1) that bracket the isomer I series reported previously by Coe et al.<sup>20</sup> and by Verlet et al.<sup>25</sup> The Ib isomer first appears as a distinct species between  $N = 25$  and  $N = 30$ , and was assigned by Ma et al. as the cavity-bound isomer.<sup>28</sup> The key feature of this experiment is that the clusters undergo collisions with warm helium atoms *after* electron attachment and prior to storage in a cold trap, which presumably removes the metastable species present under other experimental conditions.<sup>28</sup>

In an effort to measure the VDE of the bulk species directly, four different groups have recently measured the VDE of bulk-like  $e^-(\text{aq})$  in a liquid microjet, obtaining values in the range of 3.3–3.6 eV.<sup>44–47</sup> Each of these values appears to be lower than the extrapolated value of the cold isomer Ib data, which

Ma et al.<sup>28</sup> tentatively place at  $\approx 4$  eV. Together, these experiments establish a range of 3.3–4.0 eV for the bulk VDE.

Just as the experimental  $(\text{H}_2\text{O})_N^-$  isomer distribution is sensitive to source conditions,<sup>25</sup> so too is the isomer distribution obtained from simulations, which further complicates analysis and interpretation of the cluster experiments. Several recent simulations have demonstrated that electron attachment to warm, neutral water clusters tends to yield more strongly bound isomers than does attachment to cold clusters,<sup>48–50</sup> which implies that the ensuing dynamics are not ergodic, at least not on time scales that are accessible to quantum/classical simulations. This builds on earlier evidence from Jordan and co-workers<sup>39,51</sup> indicating that the experiments of Johnson and co-workers do not sample a thermal ensemble.

**1.3. Overview of the Present Work.** As should be clear from the preceding discussion, the VDE is an important experimental observable and point of contact with theoretical predictions, although the VDE alone is insufficient to determine the nature of the electron binding motif. Most previous theoretical studies of  $(\text{H}_2\text{O})_N^-$  cluster VDEs have employed one-electron models whose accuracy for computing VDEs is insufficient<sup>9,11,52</sup> to provide a meaningful *direct* comparison to experimental VDEs, although the size-dependent *trends* obtained in these calculations have provided some insight. In contrast to these pseudopotential-based simulations, Jungwirth and co-workers<sup>48,49,53</sup> have reported simulations of  $(\text{H}_2\text{O})_{32}^-$  based on ab initio molecular dynamics using density functional theory. These simulations are necessarily restricted to short time scales and clusters not substantially larger than  $N = 32$ , which is daunting in view of the sensitivity to initial conditions.

Here, we present something in between. We have developed a one-electron pseudopotential model that treats both water–water and electron–water polarization in a self-consistent fashion.<sup>52,54</sup> The latest version of this model,<sup>52</sup> which is the one used exclusively here, affords VDEs with a statistical accuracy of  $\sim 0.1$  eV, based on comparison to ab initio benchmarks ranging from  $N = 2$  to  $N = 32$ . This model also provides reasonable estimates of the properties of the bulk hydrated electron,  $e^-(\text{aq})$ , including the cavity radius, radius of gyration of the unpaired electron, and the line shape and absorption maximum of the optical spectrum.<sup>52</sup> Here, we use this model to simulate the dynamics of  $(\text{H}_2\text{O})_N^-$  clusters, ranging from  $N = 20$  to  $N = 200$ , at temperatures  $T = 100$  and  $200$  K, under various initial conditions. For  $N \geq 40$ , we observe four different isomer types that are at least metastable. On the basis of size-dependent trends in the cluster VDEs, electronic radii of gyration, and optical absorption maxima, we propose assignments for the various data series observed in photoelectron experiments.

## 2. COMPUTATIONAL METHODS

The polarizable electron–water pseudopotential (PEWP) model that we employ was first described in ref 54 but subsequently re-parameterized in ref 52. Our model is best understood as a hybrid quantum mechanics/molecular mechanics (QM/MM) model with a one-electron QM region (represented here using a  $30 \times 30 \times 30$  cubic grid with a grid spacing  $\Delta x = 1.03$  Å). The MM water molecules are described by a polarizable force field,<sup>55</sup> wherein polarization is represented in terms of inducible dipoles,  $\vec{\mu}_i$ . The QM Hamiltonian depends parametrically on these dipoles, hence, the Schrödinger equation

$$\left( -\frac{\hbar^2}{2m_e} \hat{\nabla}^2 + V_{\text{elec-water}} + V_{\text{MM}} \right) |\psi\rangle = E|\psi\rangle \quad (2)$$

must be solved in conjunction with the linear-response equation for the induced dipoles,

$$\vec{\mu}_i = \alpha_i (\vec{F}_i^{\text{MM}} + \vec{F}_i^{\text{QM}}) \quad (3)$$

In eq 3,  $\alpha_i$  is the polarizability of the  $i$ th MM site and the quantities  $\vec{F}_i^{\text{MM}}$  and  $\vec{F}_i^{\text{QM}}$  represent the QM and MM contributions to the electric field, evaluated at site  $i$ . It can be shown that the induced dipoles defined by eq 3 minimize  $E$  with respect to variations in  $\vec{\mu}_i$ .<sup>54,56</sup> The Hamiltonian in eq 2 consists of a polarizable water–water force field,<sup>55</sup>  $V_{\text{MM}}$ , and an electron–water pseudopotential,<sup>52</sup>  $V_{\text{elec-water}}$ , that prevents the wave function from collapsing into the core molecular region. Simultaneous solution of eqs 2 and 3 treats electron–water and water–water polarization in a self-consistent fashion. This PEWP model has been shown to reproduce ab initio VDE benchmarks to an accuracy of  $\sim 0.1$  eV and relative energies of  $(\text{H}_2\text{O})_N^-$  and  $(\text{H}_2\text{O})_N^-$  clusters to within  $\sim 1$  kcal/mol.<sup>52</sup>

We propagate constant-temperature molecular dynamics using a velocity Verlet/Nosé-Hoover algorithm,<sup>57</sup> with a time step of 0.5 fs. As detailed in ref 52, the grid must be translated during the simulation in order to prevent the wave function from reaching the edge, which can lead to a small drift in the total (system + bath) energy. For the simulations reported here, however, the temperature is well conserved and the total energy is conserved to within the fluctuations of the system  $[(\text{H}_2\text{O})_N^-]$  energy.

Simulations were performed for  $N = 20, 40, 60, 80, 100,$  and  $200$ , at temperatures  $T = 100$  and  $200$  K. For each  $N$  and  $T$ , two simulations were performed with different initial conditions. In what we will call the “cavity-initialized” simulation, the initial geometry was extracted from a previous simulation<sup>52</sup> of  $e^-(\text{aq})$  in bulk water at  $T = 300$  K, and initial velocities were sampled from a Maxwell–Boltzmann distribution at the target temperature. In a second, “neutral-initialized” simulation, the initial cluster geometry was extracted from a simulation of neat liquid water at  $T = 300$  K, and then instantaneously adjusted to the target temperature (100 or 200 K); the neutral cluster was then equilibrated for 100 ps prior to electron attachment.

At  $T = 100$  K, the cluster probably lacks sufficient energy to anneal, and the equilibrated geometries that we obtain are most likely metastable. At  $T = 200$  K, however, significant arrangement is still possible. These temperatures were chosen to approximate, or at least bracket, a relevant temperature for the photoelectron experiments of Neumark and co-workers.<sup>25</sup> Our decision not to anneal the neutral geometries more carefully is discussed below, and relates to recent work by Rossky and co-workers<sup>50</sup> as well as by Jungwirth and co-workers<sup>48,49</sup> demonstrating a sensitivity to initial conditions. Several additional, shorter trajectories were used to evaluate this issue and will be discussed in Section 3.1.

Structures were recorded every 10 fs for analysis, and snapshots were taken every 500 fs to compute absorption spectra, except for the shorter trajectories where snapshots are taken every 100 fs. Because the inducible dipoles  $\vec{\mu}_i$  represent electronic degrees of freedom, they should relax on the time scale of electronic excitation. We compute this electronic relaxation of the solvent in a perturbative fashion, as described in previous work.<sup>52,58</sup> A self-consistent treatment of electronic reorganization in the solvent has only a moderate affect on the overall absorption line shape, and does not affect the absorption maximum.<sup>59</sup>

## 3. RESULTS

**3.1. Observed Isomer Types.** To differentiate between surface and cavity isomers, we require some metric that tells us where the excess electron is located relative to the surface of the cluster. In previous studies,<sup>29,60</sup> such a metric has been devised in terms of the radius of gyration of the water cluster,  $R_{\text{gyr}}^{\text{clust}}$ , the radius of

gyration of the one-electron wave function,  $R_{\text{gyr}}^{\text{elec}}$ , and the distance from the electron to the cluster,  $|\vec{R}_{\text{elec}} - \vec{R}_{\text{clust}}|$ . (Here,  $\vec{R}_{\text{elec}}$  represents the centroid of the wave function and  $\vec{R}_{\text{clust}}$  is either the center of mass or else the centroid of the water cluster.) If

$$|\vec{R}_{\text{elec}} - \vec{R}_{\text{clust}}| + R_{\text{gyr}}^{\text{elec}} < R_{\text{clust}}^{\text{surf}} \quad (4)$$

then it is reasonable to call the isomer in question a cavity isomer, because on average the wave function does not extend beyond the surface of the cluster.

Although the metric in eq 4 is reasonable, we have found it useful to take into account the potentially nonspherical nature of the cluster. To do so, we approximate the shape of the cluster as an ellipsoid defined by

$$\frac{x^2}{A^2} + \frac{y^2}{B^2} + \frac{z^2}{C^2} = 1 \quad (5)$$

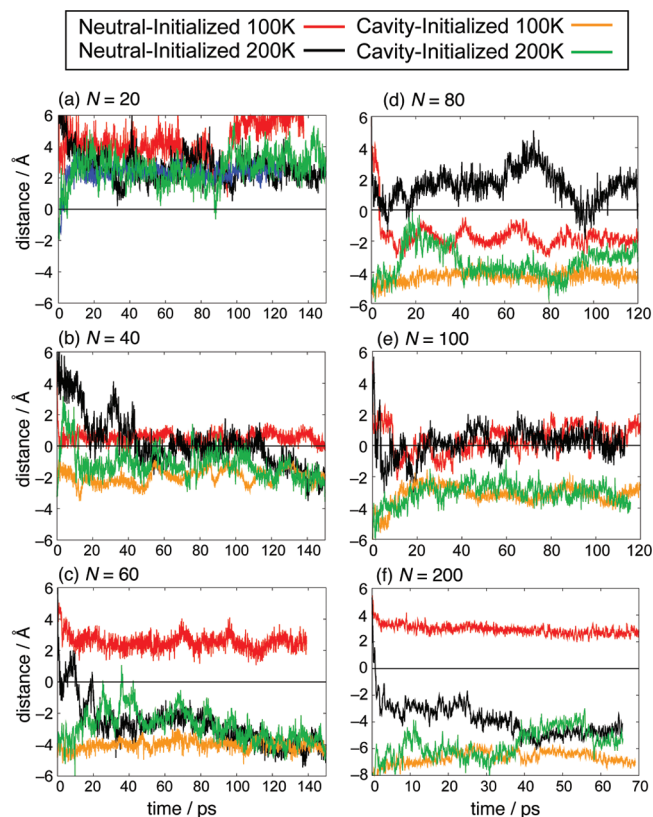
To determine the value for the parameter  $A$ , we first search the instantaneous geometry for the maximum distance between a water molecule and the centroid of the water cluster in both the positive and negative  $x$  directions. We then set  $A$  to be the average of these two distances. The parameters  $B$  and  $C$  are defined similarly. This gives a simple but reasonable description of the surface of the cluster. We then find the vector  $\vec{R}_{\text{elec}} - \vec{R}_{\text{clust}}$  that connects the centroid of the electronic wave function and the centroid of the cluster, as well as the point  $\vec{R}_{\text{surf}}$  at which this vector crosses the surface of the ellipsoid defined in eq 5. Finally, as a metric to discriminate between surface and internal isomers, we use the distance

$$d_{\text{e-surf}} = \begin{cases} -|\vec{R}_{\text{elec}} - \vec{R}_{\text{surf}}| + R_{\text{gyr}}^{\text{elec}} & \text{if } \vec{R}_{\text{elec}} \in V_{\text{ellipse}} \\ |\vec{R}_{\text{elec}} - \vec{R}_{\text{surf}}| + R_{\text{gyr}}^{\text{elec}} & \text{if } \vec{R}_{\text{elec}} \notin V_{\text{ellipse}} \end{cases} \quad (6)$$

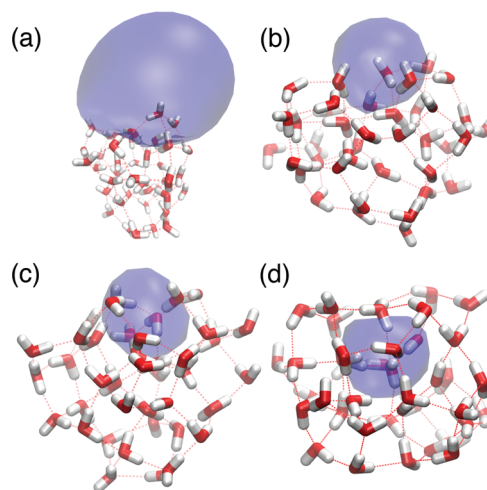
Note that  $d_{\text{e-surf}} > 0$  if the centroid of the wave function lies outside of the ellipse defined in eq 5.

Figure 2 shows the fluctuations in  $d_{\text{e-surf}}$  over the length of the simulations, for both the neutral-initialized and the cavity-initialized simulations. We consider the cavity-initialized simulations first. Among these, only for  $N = 20$  does the electron escape to create a surface isomer ( $d_{\text{e-surf}} > 0$ ); the  $N = 40$  simulation flirts with forming a surface isomer, but ultimately  $d_{\text{e-surf}} < 0$  on average. For the larger cavity-initialized clusters at  $T = 100$  K, the electron never reaches the surface and therefore does not have the opportunity to escape the cavity. At  $T = 200$  K, however, the electron is able to diffuse to the surface, and in the  $N = 60$  and  $N = 80$  clusters at  $T = 200$  K, the electron appears to find the surface within 20–40 ps but then diffuses back toward the center of the cluster, where it appears to equilibrate. This suggests that, according to our model, once a stable cavity is formed in a cluster with  $N \geq 40$ , there is a significant barrier for escape of the electron to the surface.

The neutral-initialized simulations are more interesting. All of these simulations start from a neutral structure where the electron is weakly bound, such as that depicted in Figure 3a. We refer to isomers such as that in Figure 3a as “dipole-bound”, since the vector  $\vec{R}_{\text{elec}} - \vec{R}_{\text{clust}}$  lies within  $26^\circ$  of the cluster dipole moment vector in these cases. Although a detailed examination of the solvation dynamics following electron attachment is beyond the scope of this work, it is worthwhile pointing out a few observations. First, the localization of the electron from weakly



**Figure 2.** Distance,  $d_{\text{e-surf}}$  (eq 6), between the excess electron and the surface of the water cluster, in various  $(\text{H}_2\text{O})_N^-$  simulations. These simulations are initialized either from an equilibrated neutral cluster or else from a cavity state extracted from a bulk  $\text{e}^-(\text{aq})$  simulation. Note that some panels use different horizontal and/or vertical scales.



**Figure 3.** Examples of the four isomer types observed in this work, for the case of  $(\text{H}_2\text{O})_{40}^-$ : (a) a dipole-bound surface isomer, (b) a proper surface isomer, (c) a partially embedded surface isomer, and (d) a cavity isomer. The isosurfaces that are shown encapsulate 70% of the electron density.

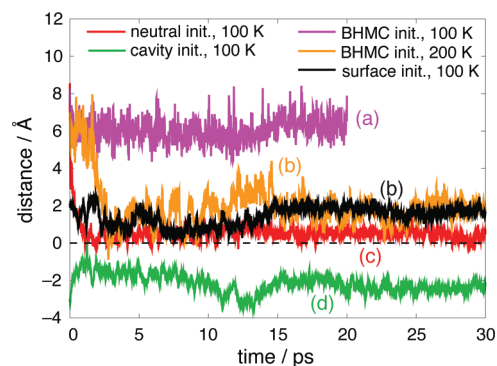
to strongly bound ( $\text{VDE} > 1.0$  eV) is rapid, and in all cases, this initial localization occurs via a reorientation of dangling O–H moieties on the surface of the cluster, so that they point toward the excess electron. Once the electron is bound by several directed

O–H groups, we observe two possible pathways through which the electron can transition to a stronger binding motif. First, it may happen that three or more dangling O–H moieties are in close enough proximity that they can form a sort of pseudo-cavity, without disrupting hydrogen bonding near the electron, similar to the geometry shown in Figure 3b. Alternatively, thermal fluctuations in the hydrogen-bonding network may cause a dangling O–H near the electron to break its only hydrogen bond. If this occurs near the electron, then this water molecule can rotate toward the centroid of the electron and form an AA binding motif, which can more strongly localize the electron. The clusters studied here are large enough so that there are typically several dangling O–H groups near the excess electron, and if an AA forms, it is not the sole participant in solvating the electron. Once the electron is sufficiently localized, O–H groups with disrupted hydrogen bonds tend to orient toward the electron, or from another point of view, the electron is attracted toward O–H groups with broken hydrogen bonds. For this reason, hydrogen-bond fluctuations enable the water cluster to solvate the electron, pulling it into a pseudo-cavity at the surface of the cluster, as in Figure 3c, or in some cases fully solvating the electron as shown in Figure 3d.

Although simulations initialized from neutral water geometries can form stable surface isomers, at  $T = 200$  K the clusters with  $N = 40, 60,$  and  $200$  do spontaneously form cavity isomers, and at  $T = 100$  K the  $N = 80$  cluster also formed a cavity isomer. Although we do not have nearly enough data to estimate relative free energies for the cavity and surface isomers, our simulations certainly suggest that cavity isomers can form from surface isomers at these temperatures. At both temperatures, the  $N = 40$  and  $N = 100$  clusters form surface states with  $d_{e-surf} \approx 0$ , which implies that the centroid of the electron's wave function lies below the surface by a distance of  $R_{gyr}^{elec}$ . We refer to these as “partially-embedded” isomers. These isomers are to be contrasted with those formed at  $T = 100$  K with  $N = 20, 60,$  and  $200$ , in which the centroid is located at or above the nominal surface of the cluster. At  $T = 200$  K, the  $N = 80$  cluster appears to fluctuate between these two isomer types.

The fact that the  $N = 80$  cluster forms a cavity isomer so readily at  $T = 100$  K, whereas  $d_{e-surf}$  shows considerable variation for  $N = 80$  at  $200$  K, suggests that the initial  $(H_2O)_N$  geometries in the neutral-initialized simulations are metastable. Other studies have noted that the time-dependent VDE is strongly dependent on the initial geometry of the cluster.<sup>48–50</sup> To confirm this observation with our model, as well as to better sample the surface states, we have run a number of shorter trajectories starting from stable neutral clusters. Initial geometries were obtained by performing  $10^4$  basin-hopping Monte Carlo (BHMC) steps<sup>61</sup> at  $N = 20, 40, 60,$  and  $80$ , in order to locate stable minima. (This is unlikely to be sufficient sampling to locate the global minimum of the neutral clusters, but it does at least provide very stable neutral clusters.) These “basin-hopping initialized” geometries were then equilibrated at  $T = 100$  K for  $5$  ps prior to electron attachment. Following electron attachment, the simulations were propagated for  $20–30$  ps, after which we instantaneously increased the temperature to  $200$  K and propagated dynamics for another  $20–30$  ps. Another set of simulations were initiated by carving smaller clusters from random snapshots extracted from the  $N = 200$  surface state at  $100$  K [corresponding to the data shown in Figure 2f]. Smaller clusters with  $N = 20, 40, 60, 80,$  and  $100$  were extracted at  $100$  K and then propagated for  $20–30$  ps. We will refer to these simulations as “surface initialized”.

We will not show all of the data from these additional simulations, but as an illustrative example, we show the fluctuations



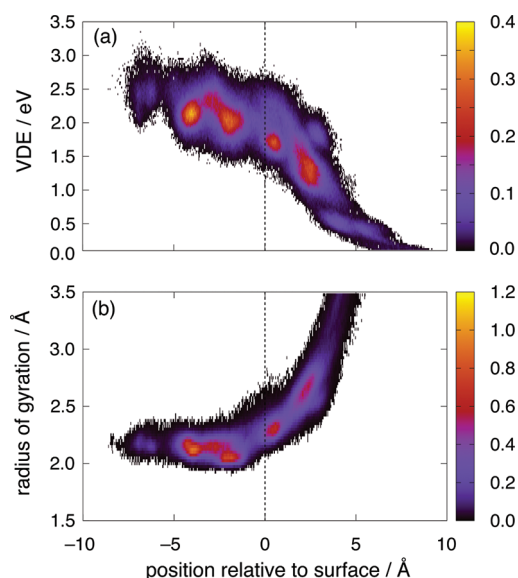
**Figure 4.** Position of the excess electron from the surface,  $d_{e-surf}$ , for a  $(H_2O)_{40}$  cluster. The labels (a)–(d) indicate that the structures correspond to one of the four isomers depicted in Figure 3.

in  $d_{e-surf}$  for the  $N = 40$  simulations, in Figure 4. Each of the data series is labeled (a)–(d), indicating that the data correspond to one of the isomer types depicted in Figure 3. (The  $N = 40$  example is useful because all four isomer types can be observed for this particular cluster size.) Electron attachment to the initial geometries from BHMC yields dipole-bound states such as that shown in Figure 3a, with little subsequent rearrangement. The simulations starting from a preformed surface state (“surface initialized”) maintain a surface-bound geometry in which the centroid of the electron is located at or above the surface of the cluster. In these cases,  $d_{e-surf} > 0$ , reflecting the fact that most of the electron density is exterior to the cluster. This is in contrast to the partially embedded isomers obtained from the neutral-initialized simulations, in which the centroid of the electron is below the surface but the average extent of the electron is still near the surface (Figure 3c). We still consider these isomers to be surface isomers since the electron is not fully solvated. For these isomers,  $d_{e-surf} \approx 0$ . Finally, Figure 3d shows a representative example of a cavity isomer in which the electron is fully solvated.

The initial dynamics in our simulations may be unrealistic, since the electron attaches to the cluster in the ground state and remains there, adiabatically. Nonetheless, the fact that differing initial geometries give rise to different, but evidently quite stable, isomers is in agreement with previous calculations.<sup>48–50</sup> It appears that electron attachment to very cold clusters (prepared with BHMC) yields weakly bound isomers, whereas attachment to warm clusters, or to metastable geometries (as in the neutral-initialized simulations) produces strongly bound isomers. This is also in agreement with the experimental observation that increasing the backing pressure in a molecular beam leads to production of more weakly bound isomers.<sup>25</sup> This implies that the simulations are not ergodic.

**3.2. Statistical Correlations among Observables.** In this section, we investigate the extent to which the VDE, the electron's radius of gyration, and the electronic absorption maximum are correlated with  $d_{e-surf}$ , the position of the electron relative to the surface of the water cluster. We estimate the absorption maximum as the average of the lowest three excitation energies, weighted by their oscillator strengths,  $f_{0,i}$ :

$$E_{\max} = \frac{\sum_{i=1}^3 (E_i - E_0) f_{0,i}}{\sum_{i=1}^3 f_{0,i}} \quad (7)$$

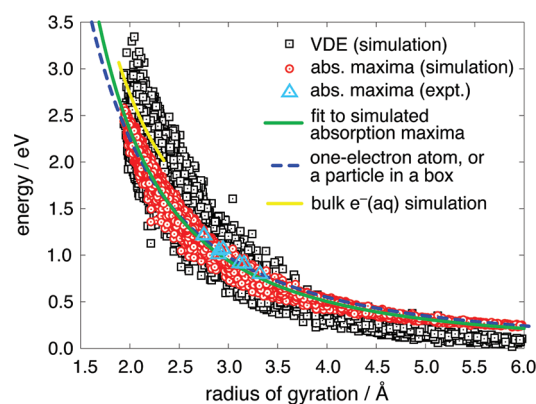


**Figure 5.** Two-dimensional probability distributions that correlate  $d_{e\text{-surf}}$ , the distance of the electron from the surface of the cluster, with either (a) the vertical detachment energy, or (b) the electron's radius of gyration. For visual clarity, near-zero values of the probability distribution have been replaced with a white background.

The three lowest excited states of the hydrated electron are nominally  $s \rightarrow p$  transitions and carry the majority of the oscillator strength.<sup>3,11,30,52,58</sup> As such, eq 7 affords a reasonable estimate of the absorption maximum.

Figure 5a shows a joint probability distribution of the VDE and  $d_{e\text{-surf}}$  for all of the simulation data, irrespective of cluster size or initial conditions. The data indicate that when the centroid of the electron is exterior to the cluster surface ( $d_{e\text{-surf}} > 0$ ), the VDE is strongly correlated with distance and grows larger as the electron approaches the surface. For a fixed value of  $d_{e\text{-surf}} > 0$ , the distribution of VDEs is narrow when  $d_{e\text{-surf}}$  is large, but broadens considerably as the  $d_{e\text{-surf}} \rightarrow 0$ , that is, as the electron approaches the surface of the cluster. For  $d_{e\text{-surf}} \approx 0$ , the electron is fully solvated and we note that correlation between  $d_{e\text{-surf}}$  and the VDE is less strong and the distribution of VDEs is fairly broad. For  $d_{e\text{-surf}} < 0$ , the VDE increases somewhat as the electron moves toward the center of the cluster. (However, this increase is at least partially artificial, because only in large clusters can the electron penetrate deeply into the cluster.)

A joint probability distribution for  $d_{e\text{-surf}}$  and  $R_{\text{gyr}}^{\text{elec}}$  is shown in Figure 5b. At positions where the centroid of the electron is exterior to the surface of the cluster, the radius of gyration contracts as the electron approaches the surface. At distances far from the surface, the radius of gyration is strongly dependent on distance, but this dependence is less dramatic near the surface. Around  $d_{e\text{-surf}} = 0$  there is a dramatic change, and  $R_{\text{gyr}}^{\text{elec}}$  becomes nearly independent of  $d_{e\text{-surf}}$ . Evidently, once the electron becomes fully solvated, the radius of gyration stabilizes around its bulk value. (Our model predicts  $R_{\text{gyr}}^{\text{elec}} \approx 2.3 \text{ \AA}$  in bulk water at  $T = 300 \text{ K}$ ,<sup>52</sup> but this limiting value is contracted slightly in these clusters due to the colder temperature.) This observation is consistent with the notion that the electron's radius of gyration is a local property indicative of the solvation environment; once enough water molecules are available to solvate the electron, the extent of the  $e^-$  wave function converges.



**Figure 6.** Correlation between the electron's radius of gyration and its vertical detachment energy (black symbols) and electronic absorption maximum,  $E_{\text{max}}$  (red symbols), as obtained from simulation data on  $(\text{H}_2\text{O})_N^-$  clusters. The green curve is a fit (eq 10) of  $E_{\text{max}}$  values from the simulations. Experimental data for  $E_{\text{max}}$  (blue triangles) are obtained from fits<sup>62</sup> to the original cluster data reported in ref 24. The dashed blue curve represents the lowest excitation energy for a one-electron atom as a function of the electron's radius of gyration (eq 9); this curve has nearly the same analytic form as the analogous result for a particle-in-a-box potential (eq 8). Simulation results for bulk  $e^-(\text{aq})$  are from ref 63, and are fit very well by the same function used to fit the cluster  $E_{\text{max}}$  data, if this fit is simply shifted upward by 0.4 eV.

These observations suggest that as the electron approaches the surface, its radius of gyration contracts and its VDE increases. This, in turn, suggests that the VDE may be correlated with  $R_{\text{gyr}}^{\text{elec}}$ , which is confirmed by the plot of these two quantities in Figure 6. In fact, the correlation between the radius of gyration and the VDE is much stronger than the correlation between  $d_{e\text{-surf}}$  and the VDE (cf. Figure 5a); a similar correlation between the VDE and  $R_{\text{gyr}}^{\text{elec}}$  has been noted in all-electron calculations of  $(\text{H}_2\text{O})_N^-$  clusters.<sup>53</sup>

While the correlation in Figure 6 is unmistakable, the distribution of VDEs is fairly broad for any given value of  $R_{\text{gyr}}^{\text{elec}}$ , spanning a range of more than 1 eV when  $R_{\text{gyr}}^{\text{elec}} = 2.5 \text{ \AA}$ , for example. As such, the VDE cannot be predicted accurately based upon  $R_{\text{gyr}}^{\text{elec}}$  alone. The explanation for this observation is that the electron's radius of gyration is a probe of local solvation structure, as discussed above, but the VDE depends on other factors such as long-range electrostatic interactions. As such, the VDE increases with increasing cluster size, even for a roughly constant value of  $R_{\text{gyr}}^{\text{elec}}$ . This point is discussed in more detail in the next section.

In Figure 6, we have also plotted the electronic absorption maximum ( $E_{\text{max}}$ , as computed using eq 7) versus  $R_{\text{gyr}}^{\text{elec}}$ , for all cluster sizes. This distribution is surprisingly narrow, and therefore, unlike the case of the VDE, one *could* use  $R_{\text{gyr}}^{\text{elec}}$  to predict  $E_{\text{max}}$  to within a few tenths of an eV, regardless of the fact that a wide range of cluster sizes are represented in the data.

A strong correlation between  $R_{\text{gyr}}^{\text{elec}}$  and the average  $s \rightarrow p$  excitation energy has also been noted in one-electron pseudopotential simulations of  $e^-(\text{aq})$  in bulk water,<sup>63</sup> albeit over a narrower energy range than what is sampled in clusters. If we shift our fit of the cluster  $E_{\text{max}}$  data by 0.4 eV, we obtain a curve in good agreement with the bulk  $e^-(\text{aq})$  simulation data from ref 63. This shifted fit is shown in Figure 6. The magnitude of our empirical shift is reasonably consistent with the 0.7 eV blue shift in the simulated optical spectrum of  $e^-(\text{aq})$ , relative to experiment, that is reported in ref 63.

Also plotted in Figure 6 are seven experimental data points where a  $(\text{H}_2\text{O})_N^-$  absorption spectrum has been measured,<sup>24</sup> fit to a line shape function, and the corresponding radius of gyration determined using moment analysis.<sup>62</sup> These data points fall on precisely the same curve that we obtain from a fit to our simulation data, indicating that our potential reproduces the correct absorption maximum for a particular  $R_{\text{gyr}}^{\text{elec}}$ , according to moment analysis.

Given the strong correlation between  $E_{\text{max}}$  and  $R_{\text{gyr}}^{\text{elec}}$  that is observed in both  $e^-$  (aq) simulations (ref 63) and  $(\text{H}_2\text{O})_N^-$  simulations (this work), and which agrees with available experimental results for clusters, it is worth considering the origin of this correlation. The simulation data in Figure 6 suggest that the absorption maximum falls off as  $(R_{\text{gyr}}^{\text{elec}})^{-2}$ , both for clusters and for bulk  $e^-$  (aq), and in the latter case, this behavior can be understood in terms of a particle-in-a-box (PIB) model.

Considering, for simplicity, a particle in a three-dimensional cubic box (rather than the “spherical box” that is arguably more appropriate for this problem<sup>3</sup>), one can derive analytic formulas for both the lowest excitation energy ( $\Delta E$ ) and the ground-state radius of gyration, each as a function of box length. The box length can then be eliminated to afford  $\Delta E$  as a function of  $R_{\text{gyr}}^{\text{elec}}$ . The result is

$$\Delta E_{\text{PIB}}(R_{\text{gyr}}^{\text{elec}}) = \frac{3(\pi^2 - 6)E_h}{8(R_{\text{gyr}}^{\text{elec}}/a_0)^2} \quad (8)$$

in atomic units.

Equation 8 does indeed fall off as  $(R_{\text{gyr}}^{\text{elec}})^{-2}$ , which provides a satisfactory explanation for the bulk  $e^-$  (aq) data in Figure 6, but the use of a PIB model is perhaps bothersome in the context of  $(\text{H}_2\text{O})_N^-$  clusters. As an alternative, we can also compute the lowest energy gap and ground-state radius of gyration for a one-electron atom, each as a function of nuclear charge. Eliminating nuclear charge between these two results, we obtain  $\Delta E$  as a function of  $R_{\text{gyr}}^{\text{elec}}$  for a hydrogen-like atom. The result is

$$\begin{aligned} \Delta E_{\text{hydrogenic}}(R_{\text{gyr}}^{\text{elec}}) &= \frac{9E_h}{8(R_{\text{gyr}}^{\text{elec}}/a_0)^2} \\ &\approx \frac{8.57 \text{ eV}}{(R_{\text{gyr}}^{\text{elec}}/\text{\AA})^2} \end{aligned} \quad (9)$$

The curve indicated in eq 9 is plotted in Figure 6 and affords a strikingly good match to the  $(\text{H}_2\text{O})_N^-$  data. Inspired by this result, we fit the cluster simulation data for  $E_{\text{max}}$  to a similar functional form, obtaining

$$\Delta E_{\text{fit}} = \frac{7.0 \text{ eV}}{(R_{\text{gyr}}^{\text{elec}}/\text{\AA} - 0.27/\text{\AA})^2} \quad (10)$$

This is the fit that is reported in Figure 6.

Recently, we have observed a similar trend when one uses time-dependent density functional theory (TD-DFT) to compute an electronic absorption spectrum (based on many-electron quantum mechanics) using geometries from one-electron pseudopotential simulations.<sup>11</sup> Geometries generated from pseudopotentials that predict a too-small value of  $R_{\text{gyr}}^{\text{elec}}$  for bulk  $e^-$  (aq), based on comparison to the value extracted from the experimental absorption line shape,<sup>62</sup> are found to afford TD-DFT spectra that are blue-shifted relative to experiment. Pseudopotential models where the predicted value of  $R_{\text{gyr}}^{\text{elec}}$  is larger than the experimentally derived value afford TD-DFT spectra that are red-shifted relative to experiment. Geometries obtained from the

Turi-Borgis pseudopotential model,<sup>30</sup> which predicts a bulk value of  $R_{\text{gyr}}^{\text{elec}}$  in quantitative agreement with experiment, afford a TD-DFT spectrum in nearly quantitative agreement with experiment.<sup>11</sup>

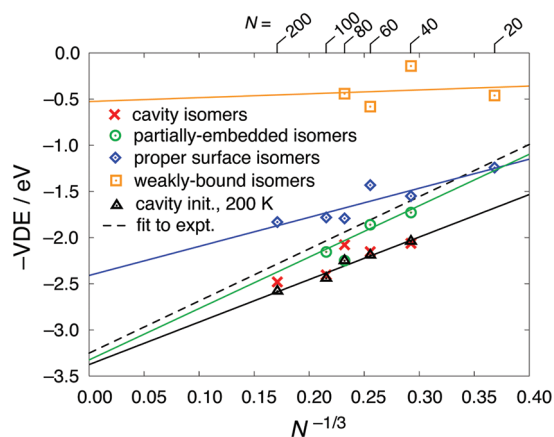
The conclusion that we draw from the preceding discussion is that the absorption maximum will not red-shift with increasing cluster size for cavity-bound isomers of  $(\text{H}_2\text{O})_N^-$  because, regardless of cluster size, once the electron is fully solvated the system samples a narrow range of possible values of  $R_{\text{gyr}}^{\text{elec}}$ . The radius of gyration is so highly correlated with the absorption maximum that the latter will not shift further, once  $N$  is large enough to fully encapsulate the cavity-bound electron. Contrariwise, when the electron is exterior to the surface, a much broader range of  $R_{\text{gyr}}^{\text{elec}}$  can be sampled, which may lead to systematic shifts of the absorption maximum as  $N$  varies. The fact that the absorption spectrum of cavity isomers does not shift with cluster size has been noted in previous simulations of  $(\text{H}_2\text{O})_N^-$  clusters,<sup>23,29,64</sup> but the data presented here provide a compelling explanation for this observation.

**3.3. Extrapolation of Vertical Detachment Energies.** To date, four different sequences of  $(\text{H}_2\text{O})_N^-$  isomers have been inferred based on photoelectron spectroscopy.<sup>25,28</sup> Neumark and co-workers<sup>25</sup> have observed three series of isomers that they labeled I, II, and III; the isomer I data are the most strongly bound, and essentially coincide with the isomer series first observed by Bowen and co-workers,<sup>20</sup> which was later extrapolated to the bulk limit.<sup>21</sup> No isomers with VDEs larger than the isomer I clusters were observed in the experimental setup of Neumark and co-workers.<sup>65</sup> More recently, however, von Issendorff and co-workers<sup>28</sup> reported two series of isomers (labeled Ia and Ib in Figure 1) that bracket the isomer I data and lie about 0.5 eV apart. These VDEs also scale linearly with  $N^{-1/3}$ , at least beyond  $N \approx 50$  where there is a change in slope.

The validity of extrapolating the isomer I data to the bulk limit has been questioned, most directly by Turi et al.<sup>29</sup> who suggest, on the basis of simulations, that these data instead correspond to surface-bound isomers. Specifically, the highest-binding isomer series in the simulations of Turi et al., which consists of surface states, reproduces the red shift seen experimentally in the absorption maximum, as a function of cluster size. In the previous section, we demonstrated that the location of the absorption maximum is proportional to the inverse square of the electronic radius of gyration, which implies that a systematic red shift is indicative of a trend toward a more localized electron. Unfortunately, the pseudopotential model employed by Turi et al.<sup>29</sup> is not sufficiently accurate in its prediction of cluster VDEs to afford a meaningful direct comparison to experimental photoelectron data, which has led to questions regarding the validity of these conclusions.<sup>31,32</sup>

In this section, we evaluate the scaling of both the VDE and  $R_{\text{gyr}}^{\text{elec}}$  as a function of cluster size. Above, we classified the isomers observed in our simulations into four types: cavity-bound isomers, partially embedded surface isomers, proper surface isomers, and dipole-bound surface isomers. The data presented in this section are averages (at a given  $N$ ) over data corresponding to each isomer type. Figure 7 plots the average VDE, as a function of  $N^{-1/3}$ , for each of these four isomer types. Cavity isomers bind the electron the most strongly, followed by partially embedded surface isomers and then proper surface isomers.

VDEs for the dipole-bound isomers are typically less than 0.5 eV, and we observe these isomers only in simulations where we attach an electron to a very cold, stable neutral cluster (the “BHMC-initialized” simulations). For these isomers, there is



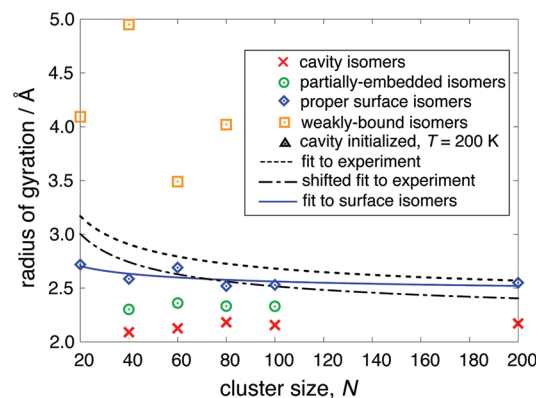
**Figure 7.** Plot of negative VDE versus  $N^{-1/3}$  for all of the  $(\text{H}_2\text{O})_N^-$  cluster data. The broken line represents an extrapolation of the experimental “isomer I” data, and is taken from ref 62.

significant scatter in the average VDE as a function of  $N$ . However, there is far less scatter for the remaining classes of isomers, and each exhibits VDEs that scale approximately linearly versus  $N^{-1/3}$ . Significantly, the cavity-bound and partially embedded surface isomers extrapolate with similar slopes.

Also shown in Figure 7 is an extrapolation<sup>62</sup> of the photoelectron data of Coe et al.,<sup>20</sup> which are quite similar to the more recent isomer I data reported by Verlet et al.<sup>25</sup> The VDEs of the partially embedded isomers are in excellent agreement with this extrapolation. The cavity isomers are bound more strongly than the partially embedded isomers by  $\approx 0.3$  eV, reminiscent of the 0.5 eV gap between the isomer Ia and isomer Ib data reported by Ma et al.<sup>28</sup> This fact supports the assignment of the isomer Ib series as cavity-bound isomers.

The key difference between the experiments of Coe et al.<sup>20</sup> and Verlet et al.,<sup>25</sup> both of which identified isomer I, and those of Ma et al.,<sup>28</sup> which identified the higher-binding isomer Ib, is that in the latter case the clusters isomers that are observed are likely more stable, as a result of the experimental setup. To make contact with this fact, we have also plotted in Figure 7 the VDEs for our cavity-initialized simulations at  $T = 200$  K. The average VDEs in these simulations are much more linear, as a function of  $N^{-1/3}$ , than are the cavity-bound VDEs in general (i.e., when averaged over all simulations and initial conditions). Moreover, the cavity-initialized simulation affords a mean VDE that is larger than the overall average, at each value of  $N$ . We interpret this as an indication that  $(\text{H}_2\text{O})_N^-$  simulations initialized from neutral cluster isomers, or at colder temperatures, are easily trapped in metastable geometries, whereas if we consider only warmer simulations that were started from equilibrated, cavity-bound cluster isomers, then the VDEs fall nicely along a straight line as a function of  $N^{-1/3}$ .

Next, we consider the  $N$ -dependence of  $R_{\text{gyr}}^{\text{elec}}$ . We use this observable in place of the absorption maximum, since it is easier to compute and, according to the discussion in Section 3.2, serves as an equally valid metric of electron localization. Figure 8 shows the variation in  $R_{\text{gyr}}^{\text{elec}}$  as a function of cluster size, and in agreement with several previous theoretical studies,<sup>23,29,64,66</sup> the cavity isomers display no shift in  $R_{\text{gyr}}^{\text{elec}}$ . (This is also clear from the correlation between  $R_{\text{gyr}}^{\text{elec}}$  and the position of the electron’s centroid, as shown in Figure 5b.) Perhaps more surprising is the fact that the partially embedded surface isomers also display no shift in  $R_{\text{gyr}}^{\text{elec}}$



**Figure 8.** Radius of gyration of the excess electron, as a function of  $N$ . The fit to experiment is based on radii of gyration obtained<sup>62</sup> from the line shapes of electronic absorption spectra measured for various  $N$ .<sup>24</sup>

as a function of cluster size, although  $R_{\text{gyr}}^{\text{elec}}$  is consistently larger (by about 0.2 Å) for the partially embedded isomers than for the cavity-bound isomers. In contrast, the surface-bound isomers do appear to exhibit a contraction of  $R_{\text{gyr}}^{\text{elec}}$  with cluster size, albeit a very slight one. Radii of gyration for the dipole-bound isomers exhibit no obvious correlation with cluster size, although  $R_{\text{gyr}}^{\text{elec}}$  is clearly larger for these isomers than for the other isomer types.

Also shown in Figure 8 is an experimental fit of the radius of gyration as a function of cluster size,<sup>62</sup> based on  $(\text{H}_2\text{O})_N^-$  electronic absorption line shapes.<sup>24</sup> This fit was designed to extrapolate cluster  $R_{\text{gyr}}^{\text{elec}}$  data to the bulk limit, and in the bulk limit this fit affords  $R_{\text{gyr}}^{\text{elec}} \approx 2.2$  Å. Our simulated  $R_{\text{gyr}}^{\text{elec}}$  values for cavity-bound isomers extrapolate to a slightly smaller value,  $R_{\text{gyr}}^{\text{elec}} \approx 2.1$  Å. Thus, Figure 8 also depicts a shifted version of the experimental fit, in which the shift (0.15 Å) is chosen so that the fit extrapolates to  $R_{\text{gyr}}^{\text{elec}} = 2.1$  Å. (The fact that such a shift is necessary is consistent with the fact that our PEWP model affords a radius of gyration for  $e^-(\text{aq})$  in bulk water that is 0.2 Å smaller than experimental estimates extracted from the absorption line shape.<sup>52</sup>) This shifted fit is in fair agreement with our simulated data for surface-bound cluster isomers.

## 4. DISCUSSION

**4.1. Possible Sources of Error.** Prior to giving an interpretation for our results, we would like to discuss the most likely sources of error in these simulations.

Our model was tested against an extensive set of ab initio VDEs for  $(\text{H}_2\text{O})_N^-$  clusters ranging from  $N = 2$  to  $N = 32$ , having VDEs ranging from  $\approx 0$  up to 2.5 eV. The mean error, with respect to the ab initio benchmarks, is less than 0.1 eV.<sup>52</sup> For this reason, we believe the VDE should be fairly accurate, for any given cluster geometry.

In the bulk, our model gives a radius of gyration that is smaller than the experimentally estimated one,<sup>62</sup> by about 0.2 Å at  $T = 298$  K.<sup>52</sup> This indicates that the model overlocalizes  $e^-(\text{aq})$  in a too-small solvent cavity, which is corroborated by the fact that we have to shift the experimental fit of the cluster  $R_{\text{gyr}}^{\text{elec}}$  data in Figure 8 by about 0.15 Å in order to match our simulated data for surface-bound isomers. (This fit was performed for  $T = 210$  K,<sup>62</sup> where  $R_{\text{gyr}}^{\text{elec}}$  is smaller than at 298 K; hence, the overlocalization observed here is a bit less than in our previous bulk simulations at  $T = 298$  K.)



We expect that there is an energetic cost to cavity formation that grows in proportion to the surface area of the cavity, that is, it should increase as  $R_{\text{gyr}}^{\text{elec}}$  increases. Together with the observation that the PEWP model predicts cavities that are slightly too small, this provides at least a partial explanation as to why we observe spontaneous formation of cavity isomers at  $N \sim 40$ , whereas the model due to Turi and Borgis<sup>30</sup> predicts that cavity isomers will spontaneously isomerize into surface-bound isomers, even in clusters considerably larger than  $N = 40$ .<sup>29</sup> At present, we lack sufficient information to determine whether this is the sole reason why the surface  $\rightarrow$  internal transition occurs in smaller clusters with our model, although based on the fact that our model compares favorably to ab initio predictions of the relative energies of both neutral and anionic water clusters,<sup>52</sup> we suspect that there is more to it than this. Investigation of free energies of solvation would be a useful avenue of future research and may aid in understanding the differences in the behavior of these two models.

The fact that different initial conditions lead to different final geometries, radii of gyration, and VDEs suggests that the dynamics are not ergodic, at least not on the time scales simulated here. This is also borne out of the experimental data, specifically, the fact that the proportion of isomer types seen experimentally can be modified by adjusting the initial conditions.<sup>25</sup> As such, an additional source of error in these calculations is the poor sampling of initial conditions. We have studied seven different types of initial conditions for  $N = 20, 40, 60$ , and  $80$ , with fewer assorted initial conditions for  $N = 100$  and  $200$ . This is of course a minute fraction of all possible initial conditions. For this reason, it is best not to assume a one-to-one correspondence between our simulated isomers and those that have been observed experimentally. Better sampling of initial conditions is an additional avenue of research, which has been explored recently using a different pseudopotential model.<sup>50</sup>

**4.2. Interpretation.** In our simulations, only the surface isomers display a contraction in  $R_{\text{gyr}}^{\text{elec}}$  as a function of cluster size. Since the absorption spectra taken by Ayotte and Johnson<sup>24</sup> blue-shift with increasing cluster size, we conclude that our model supports the assignment of isomer Ia as surface-bound isomers. Prior to the first report of the isomer Ia photoelectron data,<sup>28</sup> Turi et al.<sup>29</sup> assigned the isomer I data to surface states. This assignment is consistent with our interpretation, for  $N \lesssim 35$ , but in larger clusters, the isomer I and Ia data series diverge from one another, which may indicate a size-dependent structural transition in at least one of these two data sets.

Interestingly, the extrapolation of the VDE data for isomer I reported by Coe et al.<sup>62</sup> falls in between our predicted VDEs for proper surface isomers and partially embedded surface isomers (see Figure 7). At the same time, the shifted  $R_{\text{gyr}}^{\text{elec}}$  extrapolation shown in Figure 8 starts, for small  $N$ , with  $R_{\text{gyr}}^{\text{elec}}$  more diffuse than the values that we obtain for proper surface states in our simulations, but by  $N = 200$  this extrapolation lies very close to the value of  $R_{\text{gyr}}^{\text{elec}}$  that we obtain from simulations of the partially embedded isomers.

Figure 5b shows that  $R_{\text{gyr}}^{\text{elec}}$  is strongly correlated with the distance between the centroid of the  $e^-$  wave function and the surface of the cluster, provided that the centroid is exterior to the surface, while Figure 8 shows that the contraction of  $R_{\text{gyr}}^{\text{elec}}$  within a given isomer type is slight. This makes sense because we have categorized isomers based on the distance between the centroid and the surface, a logical metric. One interpretation of these observations is that the isomer I data do not directly correspond to either our simulated surface-bound isomers or partially embedded isomers,

but instead to some combination. That is, isomer I may represent a slow trend toward tighter binding of the electron, converging not to cavity states but rather to partially embedded surface states.

This interpretation potentially explains several interesting features of the isomer I photoelectron data. First, these data display a kink around  $N = 30$  (see Figure 1), as do the excited-state lifetimes measured by Neumark and co-workers,<sup>26,67–69</sup> which agree with bulk measurements when extrapolated to  $N = \infty$ . These observations may indicate a change from weakly bound surface isomers to more cooperatively bound, partially embedded surface isomers. It is possible that the solvation dynamics of the partially embedded isomers might be quite similar to a true cavity isomer; this should be investigated in the future.

It is worth noting that the isomer Ia data reported by Ma et al.<sup>28</sup> do *not* exhibit a kink around  $N = 30$  but rather continue on a straight line versus  $N^{-1/3}$ , in contrast to the isomer I data. In larger clusters, the isomer I data actually lie between the isomer Ia and Ib data. This may indicate that the isomers observed by Ma et al. at very low temperatures form stable surface states (Ia) and cavity states (Ib), while the isomer I data observed by Verlet et al.<sup>25</sup> represent something in between, that is, a partially embedded surface state.

Additional experimental work may help to clarify, revise, or validate these conclusions. Previous theoretical studies concur that the absorption spectrum of cavity isomers does not shift with cluster size.<sup>23,29</sup> Experimental data regarding the absorption maxima of the isomer Ib clusters might therefore be quite illuminating, as would be an extension of the experimental data for isomer I out to larger cluster sizes ( $N > 200$ ), in order to refine the extrapolation to  $N = \infty$ . If the isomer I series does indeed undergo a transition to a partially embedded isomer, then on the basis of our simulations, one would expect the absorption maximum to converge to some value lying to the red of the bulk  $e^-$  (aq) absorption maximum.

On the theoretical side, we would like to investigate isomer sizes 10–50 in more detail to better assess whether extrapolations of  $R_{\text{gyr}}^{\text{elec}}$  or the absorption spectra match experimental extrapolations in this region. Initial conditions should be sampled further, in order to generate a larger number of isomer types or else give confidence that the four reported here are indeed representative. The excited-state relaxation dynamics of surface, partially embedded, and cavity states should be investigated and compared. The free energy of solvation for the hydrated electron should be investigated in order to understand energy differences between the isomer types, and how the distribution of isomers is affected by the choice of one-electron pseudopotential model.

## 5. SUMMARY

We have employed a polarizable electron–water pseudopotential model to investigate  $(\text{H}_2\text{O})_N^-$  clusters using mixed quantum/classical molecular dynamics. Four distinct classes of isomers are observed in these simulations: dipole-bound clusters, in which the electron is weakly bound at the positive end of the  $(\text{H}_2\text{O})_N$  cluster dipole moment; “proper” surface isomers, in which the electron binds more strongly but is still largely excluded from the interior of the cluster; partially embedded surface isomers; and fully embedded cavity-type isomers, in which the electron is fully solvated.

Regardless of the particular isomer in question, we find that the radius of gyration of the excess electron contracts as the centroid of its wave function approaches the surface of the

cluster, but once the electron is fully solvated, the radius of gyration does not contract as a function of cluster size. The radius of gyration is found to be highly correlated with the location of the optical absorption maximum, implying that the absorption maximum of cavity isomers will not shift with cluster size in the manner that is observed in experimental cluster absorption spectra.<sup>24</sup> We conclude that our results support the assignment of the isomer I photoelectron data<sup>20,25</sup> to be surface isomers of some kind, in agreement with a previous theoretical study.<sup>29</sup>

The VDEs of the proper surface isomers that we observe in our calculations extrapolate to the bulk limit with a different slope than do the VDEs of the partially embedded surface states. The latter, however, extrapolate with a slope that is quite similar to that obtained for cavity-bound isomers, and indeed the VDEs of these two isomeric species differ by only  $\sim 0.3$  eV. Simulated VDEs for the partially embedded isomers agree quite well with an extrapolation<sup>62</sup> of the photoelectron data for isomer I. The fact that the cavity isomers extrapolate with a similar slope but slightly higher VDEs, as compared to isomer I, supports the assignment of the isomer Ib data<sup>28</sup> to cavity isomers. We suggest that isomer I may, in small clusters, represent a true surface-bound isomer, while in larger clusters, this same series of VDEs may represent partially embedded surface isomers. This assignment could explain the change in slope of both the VDE and excited-state lifetime data that is observed experimentally,<sup>26</sup> while remaining consistent with the blue-shifting of the absorption spectra that is observed by Ayotte and Johnson in small clusters,<sup>24</sup> and the fact that photoelectron spectra of small clusters measured by Johnson and co-workers<sup>27</sup> under similar conditions appear to merge seamlessly with the isomer I photoelectron data.<sup>25</sup>

## ■ ASSOCIATED CONTENT

Supporting Information. Complete citation for ref 1. This material is available free of charge via the Internet at <http://pubs.acs.org>.

## ■ AUTHOR INFORMATION

### Corresponding Author

herbert@chemistry.ohio-state.edu

### Present Addresses

<sup>†</sup>Dept. of Chemistry, Yale University, New Haven, CT.

## ■ ACKNOWLEDGMENT

This work was supported by a National Science Foundation CAREER award (CHE-0748448) and calculations were performed at the Ohio Supercomputer Center under project PAS0291. J.M.H. is an Alfred P. Sloan Foundation Fellow and a Camille Dreyfus Teacher-Scholar. L.D.J. acknowledges a Presidential Fellowship from The Ohio State University.

## ■ REFERENCES

- (1) Garrett, B. C.; et al. *Chem. Rev.* **2005**, *105*, 355.
- (2) Hart, E. J.; Boag, J. W. *J. Am. Chem. Soc.* **1962**, *84*, 4090.
- (3) Herbert, J. M.; Jacobson, L. D. *Int. Rev. Phys. Chem.* **2011**, *30*, 1.
- (4) Kevan, L. *J. Phys. Chem.* **1981**, *85*, 1628.
- (5) Tauber, M. J.; Mathies, R. A. *J. Am. Chem. Soc.* **2003**, *125*, 1394–1402.
- (6) Shkrob, I. A. *J. Phys. Chem. A* **2007**, *111*, 5223.
- (7) Larsen, R. E.; Glover, W. J.; Schwartz, B. J. *Science* **2010**, *329*, 65.
- (8) Turi, L.; Madarász, A. *Science* **2011**, *331*, 1387.
- (9) Jacobson, L. D.; Herbert, J. M. *Science* **2011**, *331*, 1387.
- (10) Larsen, R. E.; Glover, W. J.; Schwartz, B. J. *Science* **2011**, *331*, 1387.
- (11) Herbert, J. M.; Jacobson, L. D. *J. Phys. Chem. A*, (in press; DOI: 10.1021/jp206391d).
- (12) Simons, J. *Acc. Chem. Res.* **2006**, *39*, 772.
- (13) Wang, C.-R.; Nguyen, J.; Lu, Q.-B. *J. Am. Chem. Soc.* **2009**, *131*, 11320.
- (14) Siefermann, K. R.; Abel, B. *Angew. Chem., Int. Ed.* **2011**, *50*, 5264.
- (15) Armbruster, M.; Haberland, H.; Schindler, H. *Phys. Rev. Lett.* **1981**, *47*, 323.
- (16) Haberland, H.; Langosch, H.; Schindler, H.; Worsnop, D. R. *J. Phys. Chem.* **1984**, *88*, 3903.
- (17) Barnett, R. N.; Landman, U.; Cleveland, C. L. *Phys. Rev. Lett.* **1987**, *59*, 811.
- (18) Barnett, R. N.; Landman, U.; Cleveland, C. L.; Jortner, J. *J. Chem. Phys.* **1988**, *88*, 4421.
- (19) Barnett, R. N.; Landman, U.; Cleveland, C. L.; Jortner, J. *J. Chem. Phys.* **1988**, *88*, 4429.
- (20) Coe, J. V.; Lee, G. H.; Eaton, J. G.; Arnold, S. T.; Sarkas, H. W.; Bowen, K. H.; Ludewigt, C.; Haberland, H.; Worsnop, D. R. *J. Chem. Phys.* **1990**, *92*, 3980.
- (21) Coe, J. V.; Arnold, S. T.; Eaton, J. G.; Lee, G. H.; Bowen, K. H. *J. Phys. Chem.* **2006**, *125*, 014315.
- (22) Makov, G.; Nitzan, A. *J. Phys. Chem.* **1994**, *98*, 3459.
- (23) Barnett, R. N.; Landman, U.; Makov, G.; Nitzan, A. *J. Chem. Phys.* **1990**, *93*, 6226.
- (24) Ayotte, P.; Johnson, M. A. *J. Chem. Phys.* **1997**, *106*, 811.
- (25) Verlet, J. R. R.; Bragg, A. E.; Kammrath, A.; Cheshnovsky, O.; Neumark, D. M. *Science* **2005**, *307*, 93.
- (26) Neumark, D. M. *Mol. Phys.* **2008**, *106*, 2183.
- (27) Kim, J.; Becker, I.; Cheshnovsky, O.; Johnson, M. A. *Chem. Phys. Lett.* **1998**, *297*, 90.
- (28) Ma, L.; Majer, K.; Chirof, F.; von Issendorff, B. *J. Chem. Phys.* **2009**, *131*, 144303.
- (29) Turi, L.; Sheu, W.-S.; Rossky, P. J. *Science* **2005**, *309*, 914.
- (30) Turi, L.; Borgis, D. *J. Chem. Phys.* **2002**, *117*, 6186.
- (31) Turi, L.; Sheu, W.-S.; Rossky, P. J. *Science* **2005**, *310*, 1769.
- (32) Verlet, J. R. R.; Bragg, A. E.; Kammrath, A.; Cheshnovsky, O.; Neumark, D. M. *Science* **2005**, *310*, 1769.
- (33) Hammer, N. I.; Shin, J. W.; Headrick, J. M.; Diken, E. G.; Roscioli, J. R.; Weddle, G. H.; Johnson, M. A. *Science* **2004**, *306*, 675.
- (34) Hammer, N. I.; Roscioli, J. R.; Johnson, M. A. *J. Phys. Chem. A* **2005**, *109*, 7896.
- (35) Hammer, N. I.; Roscioli, J. R.; Johnson, M. A.; Myshakin, E. M.; Jordan, K. D. *J. Phys. Chem. A* **2005**, *109*, 11526.
- (36) Roscioli, J. R.; Hammer, N. I.; Johnson, M. A.; Diri, K.; Jordan, K. D. *J. Chem. Phys.* **2008**, *128*, 104314.
- (37) Guasco, T. L.; Elliott, B. M.; Johnson, M. A.; Ding, J.; Jordan, K. D. *J. Phys. Chem. Lett.* **2010**, *1*, 2396.
- (38) Lee, H. M.; Lee, S.; Kim, K. S. *J. Chem. Phys.* **2003**, *119*, 187.
- (39) Sommerfeld, T.; Gardner, S. D.; DeFusco, A.; Jordan, K. D. *J. Chem. Phys.* **2006**, *125*, 174301.
- (40) Sommerfeld, T.; DeFusco, A.; Jordan, K. D. *J. Phys. Chem. A* **2008**, *112*, 11021.
- (41) Hammer, N. I.; Roscioli, J. R.; Bopp, J. C.; Headrick, J. M.; Johnson, M. A. *J. Chem. Phys.* **2005**, *123*, 244311.
- (42) Roscioli, J. R.; Hammer, N. I.; Johnson, M. A. *J. Phys. Chem. A* **2006**, *110*, 7517.
- (43) Asmis, K. R.; Santabrogio, G.; Zhou, J.; Garand, E.; Headrick, J.; Goebbert, D.; Johnson, M. A.; Neumark, D. M. *J. Chem. Phys.* **2007**, *126*, 191105.
- (44) Siefermann, K. R.; Liu, Y.; Lugovoy, E.; Link, O.; Buck, U.; Winter, B.; Abel, B. *Nature Chem.* **2010**, *2*, 274.
- (45) Tang, Y.; Shen, H.; Sekiguchi, K.; Kurahashi, N.; Mizuno, T.; Suzuki, Y. I.; Suzuki, T. *Phys. Chem. Chem. Phys.* **2010**, *12*, 3653.
- (46) Shreve, A. T.; Yen, T. A.; Neumark, D. M. *Chem. Phys. Lett.* **2010**, *493*, 216.

- (47) Lübcke, A.; Buchner, F.; Heine, N.; Hertel, I. V.; Schultz, T. *Phys. Chem. Chem. Phys.* **2010**, *12*, 14629.
- (48) Marsalek, O.; Uhlig, F.; Frigato, T.; Schmidt, B.; Jungwirth, P. *Phys. Rev. Lett.* **2010**, *105*, 043002.
- (49) Marsalek, O.; Uhlig, F.; Jungwirth, P. *J. Phys. Chem. C* **2010**, *114*, 20489.
- (50) Madarász, A.; Rossky, P. J.; Turi, L. *J. Phys. Chem. A* **2010**, *114*, 2331.
- (51) DeFusco, A.; Sommerfeld, T.; Jordan, K. D. *Chem. Phys. Lett.* **2008**, *455*, 135.
- (52) Jacobson, L. D.; Herbert, J. M. *J. Chem. Phys.* **2010**, *133*, 154506.
- (53) Frigato, T.; VandeVondele, J.; Schmidt, B.; Schütte, C.; Jungwirth, P. *J. Phys. Chem. A* **2008**, *112*, 6125.
- (54) Jacobson, L. D.; Williams, C. F.; Herbert, J. M. *J. Chem. Phys.* **2009**, *130*, 124115.
- (55) Ren, P.; Ponder, J. W. *J. Phys. Chem. B* **2003**, *107*, 5933.
- (56) Dupuis, M.; Aida, M.; Kawashima, Y.; Hirao, K. *J. Chem. Phys.* **2002**, *117*, 1242.
- (57) Martyna, G.; Tuckerman, M.; Tobias, D.; Klein, M. *Mol. Phys.* **1996**, *87*, 1117.
- (58) Jacobson, L. D.; Herbert, J. M. *J. Am. Chem. Soc.* **2010**, *132*, 10000.
- (59) Jacobson, L. D.; Herbert, J. M. *J. Chem. Theory Comput.* **2011**, *7*, 2085.
- (60) Madarász, A.; Rossky, P. J.; Turi, L. *J. Chem. Phys.* **2009**, *130*, 124319.
- (61) Wales, D. J.; Doyle, J. P. K. *J. Phys. Chem. A* **1997**, *101*, 5111.
- (62) Coe, J. V.; Williams, S. M.; Bowen, K. H. *Int. Rev. Phys. Chem.* **2008**, *27*, 27.
- (63) Rossky, P. J.; Schnitker, J. *J. Phys. Chem.* **1988**, *92*, 4277.
- (64) Madarász, A.; Rossky, P. J.; Turi, L. *J. Chem. Phys.* **2007**, *126*, 234707.
- (65) Kammrath, A.; Verlet, J. R. R.; Griffin, G. B.; Neumark, D. M. *J. Chem. Phys.* **2006**, *125*, 076101.
- (66) Bartels, D. M. *J. Chem. Phys.* **2001**, *115*, 4404–4405.
- (67) Bragg, A. E.; Verlet, J. R. R.; Kammrath, A.; Cheshnovsky, O.; Neumark, D. M. *Science* **2004**, *306*, 669.
- (68) Bragg, A. E.; Verlet, J. R. R.; Kammrath, A.; Cheshnovsky, O.; Neumark, D. M. *J. Am. Chem. Soc.* **2005**, *127*, 15283.
- (69) Griffin, G. B.; Young, R. M.; Ehrler, O. T.; Neumark, D. M. *J. Chem. Phys.* **2009**, *131*, 194302.